# Experimental investigation on water retention and tensile strength of polyacrylamide (PAM) treated saline soil

**Wei Li[1], Youcai Cao[2], Yuanhao Li[3], Quan Wang[4], Yali Wang[5], Jian Yang[6], Yiwei Jiao[7]**
[1, 2, 3, 4, 5, 6]State Grid Gansu Electric Power Company Construction Branch, Lanzhou, 730000, China
[7]School of Civil Engineering and Mechanics, Lanzhou University, Lanzhou, 730000, China
[7]Corresponding author
**E-mail:** [1]*304550629@qq.com*, [2]*1826359092@qq.com*, [3]*841497924@qq.com*, [4]*wang_quan2023@163.com*, [5]*32159680@qq.com*, [6]*1285776631@qq.com*, [7]*jiaoyiwei2025@163.com*

*Received 8 August 2025; accepted 6 March 2026; published online 16 May 2026*
*DOI https://doi.org/10.21595/jme.2026.25250*



**Abstract.** Expansive, collapsible saline soils – widespread across northwestern China – are especially susceptible to desiccation-driven shrinkage, which progressively degrades soil fabric and triggers structural damage. Here we evaluate whether water-soluble polyacrylamide (PAM) can simultaneously enhance water retention and mechanical integrity in such soils. Using Atterberg-limit characterisation, indirect tensile testing, disintegration assays and desiccation – shrinkage experiments, we show that increasing PAM concentration consistently raises the liquid limit and plasticity index, whereas the plastic limit remains largely unchanged. Both shrinkage resistance and tensile capacity exhibit a clear optimum at 0.8 % PAM, where the shrinkage limit is maximised and tensile strength reaches its peak. In agreement with these macroscopic gains, PAM substantially delays disintegration and prolongs the time to complete dispersion, indicating improved stability upon wetting. Throughout drying – spanning rapid, falling-rate and constant-rate evaporation regimes – PAM-treated soils lose water markedly more slowly, demonstrating a robust improvement in water-holding capacity. We attribute these enhancements to hydrogen bonding between amide functionalities and water molecules, polymer-chain entanglement that promotes interparticle bridging, and a reduction in particle-surface electrokinetic (zeta) potential that stabilises the soil fabric.

**Keywords:** saline soil, polyacrylamide, Atterberg limits, tensile strength, disintegration, desiccation shrinkage.

## 1. Introduction

Desiccation-induced shrinkage generates tensile stresses within soil, and micro- to macro-cracks develop once these stresses exceed the soil tensile strength [1]. In the arid and semi-arid regions of northwestern China, pronounced precipitation variability coupled with intense evaporation frequently drives desiccation-related degradation, threatening the stability of slopes, foundations and earthen relics [2], [3]. This risk is amplified for the expansive and collapsible saline soils prevalent in the region, which deteriorate more rapidly under repeated wetting-drying cycles [4]. There is therefore an urgent need for strategies that improve the physicomechanical performance of saline soils. More broadly, enhancing the resilience of underground structures to maintain operational safety under compound hazards has become a pressing societal concern [5].

Desiccation cracking and volumetric shrinkage are governed by the coupled evolution of soil water retention and tensile resistance. Accordingly, a range of fractal descriptors has been developed to quantify crack morphology [6], [7]. Extensive experiments have shown that shrinkage tends to stabilise and crack propagation ceases as the water content approaches the shrinkage limit. Morris et al. predicted crack depth using elastic parameters together with tensile and shear strengths [8]. Peron et al. reported that air-entry suction depends on the shrinkage limit

[9]. Yin et al. interpreted capillary tension in terms of changes in water-film thickness [10]. Tang et al. identified matrix suction and tensile strength as the two key mechanical parameters controlling crack initiation [11]. More recently, numerical studies have linked shrinkage and desiccation cracking directly to the hydro-mechanical behaviour of soils [12]. Zhang et al. experimentally examined the effect of NaCl concentration on desiccation cracking in bentonite and kaolin, showing that both total crack area and crack length decrease as sodium chloride concentration increases [13]. However, dedication, cracking and shrinkage behaviour in natural saline soils remain far less studied.

Polyacrylamide (PAM) is a water-soluble polymer available in non-ionic, cationic and anionic forms; the anionic variant is widely used as a flocculant [14]. To date, PAM has been applied primarily for soil-erosion control and water-saving irrigation. Levy et al. showed that PAM improves the water stability of soil aggregates [15]. Soltani-Jigheh et al. attributed agglomeration to adsorption interactions between functional groups in the PAM backbone and soil particles [16]. Deng et al. reported that PAM increases flexibility and failure strain in cement-stabilised soil [17]. Georgees et al. demonstrated strengthening of remoulded soil using unconfined compression (UCS) and repeated-load triaxial (RLT) tests [18]. Shafiqu observed that increasing PAM content enhances the compressive strength of cemented soils and reduces plastic shrinkage in cement mortar [19]. Yet, the effects of PAM on water retention and tensile strength in saline soils remain unclear.

Here we focus on naturally occurring saline soils from the Dunhuang region, a representative arid zone in northwestern China where these materials directly influence the performance of roadbeds and foundations in salt-affected ground, but where responses to PAM amendment are poorly documented. We systematically compare two indirect tensile-strength methods – Brazilian splitting and double-punch tests – to assess their applicability and limitations for this soil-polymer system. By jointly analysing Atterberg limits, tensile strength, disintegration behaviour and drying-induced water loss across a range of PAM concentrations, we identify an optimal PAM content (~0.8 wt%) that concurrently improves tensile strength, shrinkage limit, water stability and water retention capacity. Building on emerging mechanistic understanding of soil-polymer interactions, we further elucidate how PAM redistributes adsorbed and weakly bound water, thereby governing tensile behaviour from the molecular to the macroscopic scale.

## 2. Materials

The soil under investigation exists in a fluid-like state, having been formed through quaternary alluvial-proluvial deposition processes, as illustrated in Fig. 1. To precisely characterize the salinity profile of this soil, we employed ion chromatography to quantify the concentrations of soluble salts at various depths (Fig. 1(c)). Our findings reveal that the surface soil (0-0.05 m) exhibits a total salinity of 1.53 %, categorizing it as moderately saline. The dominant cation in the shallow soil stratum is calcium ($Ca^{2+}$), while chloride ($Cl^{-}$) serves as the primary anion. As we delve deeper into the soil profile, a general trend emerges where salinity decreases with increasing depth. Specifically, the salinity of the shallow layer shows a 33.3 % reduction compared to that of the soil layer at a depth of 3.0 m. Concurrently, the dominant cation undergoes a transition from ($Ca^{2+}$) to sodium ($Na^{+}$) and potassium ($K^{+}$) as depth increases. Regarding anionic composition, the order of abundance is ($Cl^{-}$) > sulfate ($SO_4^{2-}$) > bicarbonate ($HCO_3^{-}$). Notably, the concentration of ($Cl^{-}$) experiences a substantial decline with depth, whereas the levels of ($SO_4^{2-}$) and ($HCO_3^{-}$) remain relatively stable throughout the soil profile. The observed pattern of salinity variation closely mirrors the dynamics of groundwater transport within this system [19]. In this arid region, characterized by limited precipitation and intense evaporation, soluble salts carried by groundwater are continuously transported and accumulate in the shallow soil layers. This process is driven by the upward movement of groundwater due to capillary action and evaporation, which concentrates the salts near the surface. The distinct salinity gradient and ionic composition changes with depth provide valuable insights into the hydrogeochemical processes governing this

soil system, highlighting the complex interplay between groundwater movement, evaporation, and soil salinization in arid environments. Our experimental design did not systematically vary pore water chemistry with depth; all mechanical and desiccation tests were conducted on soil from the surface layer with its measured salinity and ion composition [20].

a) Surface conditions of saline-alkali soil

b) Borehole sampling profile (0-3 m)

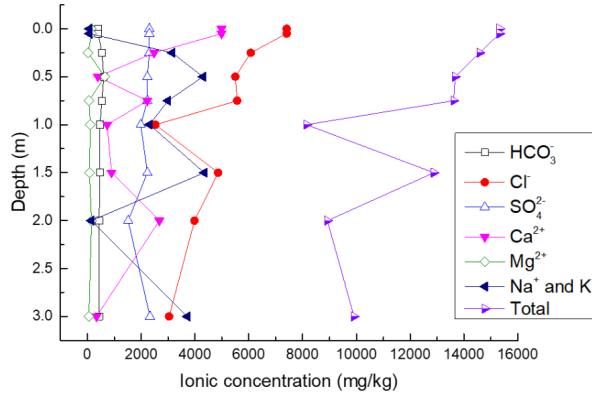


c) Ion concentrations at different depths (0–3 m)

**Fig. 1.** Salinity distribution in the study area.
Photo by Li Wei, western Gansu Province, China, May 20, 2025.

**Table 1.** Basic physical properties of saline soil

| Sample ID | Specific gravity $G_s$ | Natural moisture content (%) | Density (mg/m$^3$) | Dry density (mg/m$^3$) | Saturation (%) | Void ratio e | Compression coefficient a (MPa) |
|---|---|---|---|---|---|---|---|
| Saline soil | 2.71 | 12.2 | 1.86 | 1.66 | 60.4 | 0.5 | 0.1 |
| | Particle size grading (%) | | | | | | |
| | 0.5-0.25 mm | 0.25-0.075 mm | 0.075-0.05 mm | 0.05-0.01 mm | 0.01-0.005 mm | 0.005-0.002 mm | < 0.002 mm |
| | 12.1 | 3.2 | 3.3 | 40.1 | 32.9 | 8.4 | 0.0 |

According to Chinese "Geotechnical Testing Standard" (GB/T 50123-1999), the basic physical properties such as saturation, density etc. of soil determined by laboratory geotechnical tests are shown in Table 1. The natural moisture content is 12.2 % and compression coefficient is 0.1 MPa, indicating that the natural soil is media compressibility and rich of water. The grading of particle size shows that silt and clay fraction in shallow layer are 76.3 % and 8.4 % respectively.

The molecular formula of commercial PAM reagent used in this paper is $[-CH_2CH(CONH_2)-]_n$ (Yantai Shuangshuang Chemical Co., Ltd., China). The purity of PAM in commercial product is more than 90 %. The hydrolysis degree is 30 %, and molecular weight $>3\times10^7$. As shown in Fig. 2, the PAM solution is viscous and partially insoluble at beginning.

After 10 min stirring, the PAM reagent is dissolved.

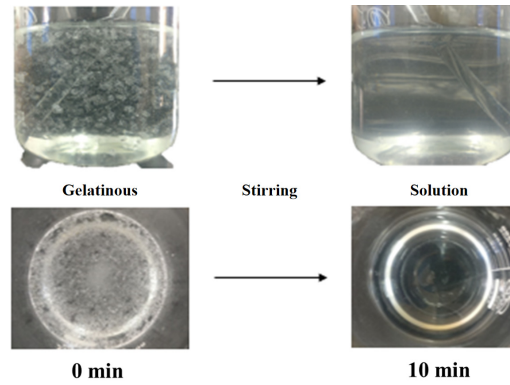


**Fig. 2.** Solubility of PAM solution. Photo by Jiao Yiwei, Lanzhou University Laboratory, Gansu Province, China, June 1, 2025

## 3. Methods

### 3.1. Atterberg limits

The air-dried saline soil was firstly screened through a 0.5 mm mesh. Then the prepared PAM solution with vary concentrations was mixed with dry soil to a uniform paste. After 24 hours sealed curing, the liquid limits (LLs) and plastic limits (PLs) of selected saline soil were determined using cone method (GYS-2, Nanjing Soil Instrument Co., Ltd., China) in accordance with Chinese standard GB/T 50123. The shrinkage limits (SLs) were determined by a contractometer (SS-1, Nanjing Soil Instrument Co., Ltd., China). After mixing air-dried soil and PAM solution to a target moisture content 15 %, and 24 hours curing to equalize moisture distribution, the samples were installed into a steel ring with a diameter of 61.8 mm and a height of 20 mm. As shown in Fig. 3(b), the correlation of linear shrinkage rate, ratio of shrinkage volume to initial volume, and moisture content was plotted. By extending the straight line of Stage I and III, the moisture content corresponding to the intersection was considered as shrinkage limit of soil [21].

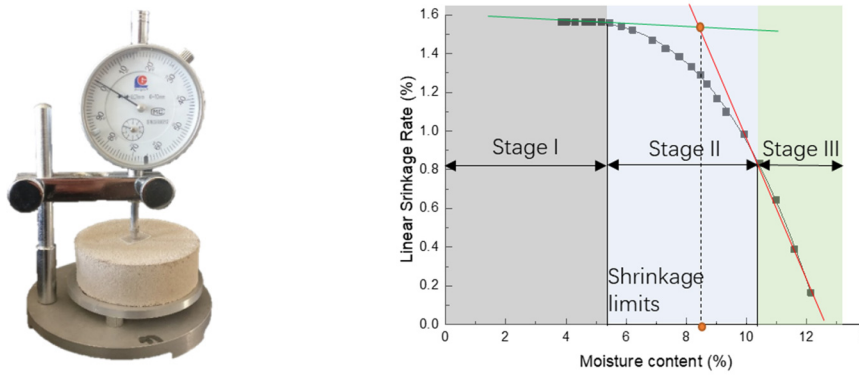


a) Set-up of contractometer SS-1 b) Diagrammatic sketch of determining shrinkage limit

**Fig. 3.** Determination of shrinkage limits.
Photo by Jiao Yiwei, Lanzhou University Laboratory, Gansu Province, China, June 2, 2025

### 3.2. Brazilian splitting and double punch tests

Two indirect methods, Brazilian splitting method (radial fracturing test) and double punch method (axial fracturing test), were adopted to determine tensile strengths of specimens (Fig. 4). After preparing a 15 % moisture content mixture of soil and PAM solution with different concentrations, the treated soil was compacted into cylindrical molds with a diameter of 39.1 mm and a height of 40 mm and a diameter of 39.1 mm and a height of 80 mm for Brazilian splitting and double punch tests respectively. Then, they were sealed and cured for 7 days. Among which, Physical sealing: Specimens were enclosed in double-layered polyethylene bags containing saturated salt solution (NaCl, relative humidity 75 %) to stabilise the microenvironment. This humidity level corresponds to the critical dissolution humidity for polyacrylamide; Temperature control: All curing occurs within a constant temperature and humidity chamber (accuracy ±0.5 °C, ±2 % RH), set at 25±1 °C (consistent with triaxial test standards), preventing accelerated moisture migration due to elevated temperatures.

As shown in Fig. 4, two rigid rods were placed parallelly along the axis direction of sample's cylindrical side for Brazilian splitting test [22]-[23]. For double punch tests, two rigid back-up blocks were placed at the top and bottom surface of cylindrical sample to conduct the vertical load [24]-[25]. The electro-hydraulic servo universal testing machine (CSS-WAW300DL, Suzhou Nanguang Electronic Technology Co., Ltd, China) was used for applying load until sample failure, and the loading speed was set as 0.8 mm/min. The maximum compression force $P$ was recorded.

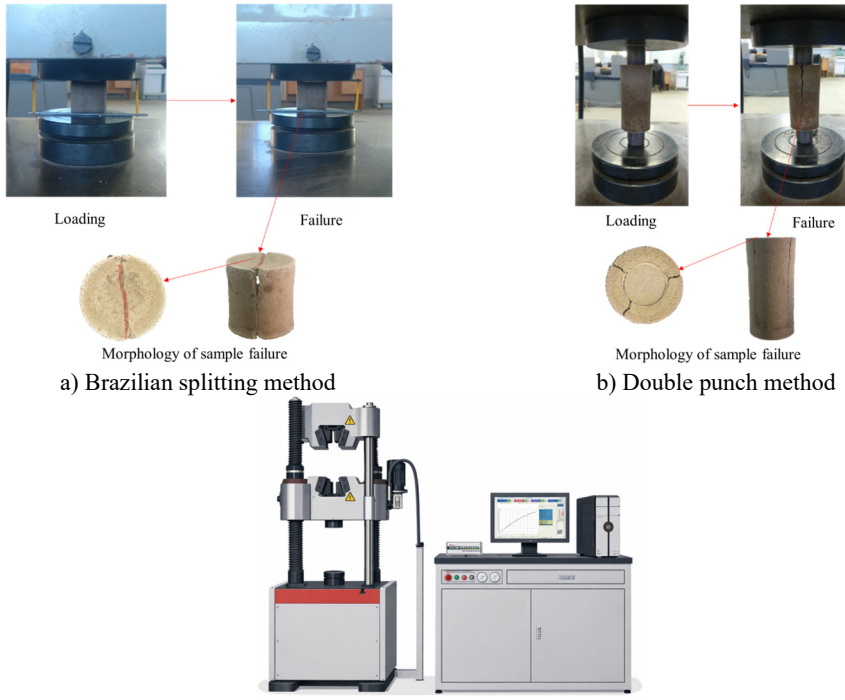


a) Brazilian splitting method b) Double punch method

c) Universal testing machine

**Fig. 4.** Set-up of tensile strength tests and appearance of sample failure.
Photo by Jiao Yiwei, Lanzhou University Laboratory, Gansu Province, China, June 6, 2025

Based on the elastic theory, Eq. (1) was used to calculate tensile strength in Brazilian splitting test:

$$\sigma_t = \frac{2P}{\pi D h}, \tag{1}$$

where $\sigma_t$ is tensile strength (MPa), $P$ is failure load (N), $D$ is diameter of specimen (mm) and $h$ is sample height (mm).

For double punch method, tensile strength was calculated from Eq. (2) according to plasticity theory:

$$\sigma_t = \frac{P}{\pi(kbh - a^2)}, \tag{2}$$

where $\sigma_t$ is tensile strength (MPa), $P$ is failure load (N), $b$ is radius of specimen (mm), $h$ is sample height (mm), $a$ is radius of back-up blocks (mm), and $k$ is a constant related to the size of rigid block and stiffness of sample. For soil, $k = 1.0$ is recommend [24].

### 3.3. Disintegration tests

According to Chinese standard SL237 [26], the set-up of disintegration test is shown in Fig. 5. The initial mass $m_0$ of 7-d cured sample was first recorded by balance. After being placed into the container for sinking, the sample was suspended under the balance and the changed mass was measured every 5 s to record the disintegration of the specimens. The disintegration ratio was calculated according to Eq. (3):

$$A_t = \frac{m_0 - m_t}{m_0 - M_1} \times 100\ \%, \tag{3}$$

where $A_t$ is cumulative disintegration ratio, $m_0$ is initial mass, $m_t$ is mass at recording time $t$ and $M_1$ is indicator of balance when sample was completely immersed in water.

The process specified by the International Organisation for Standardisation ISO/TC 147 employed in the experiment primarily utilised reverse osmosis (RO) to produce deionised water.

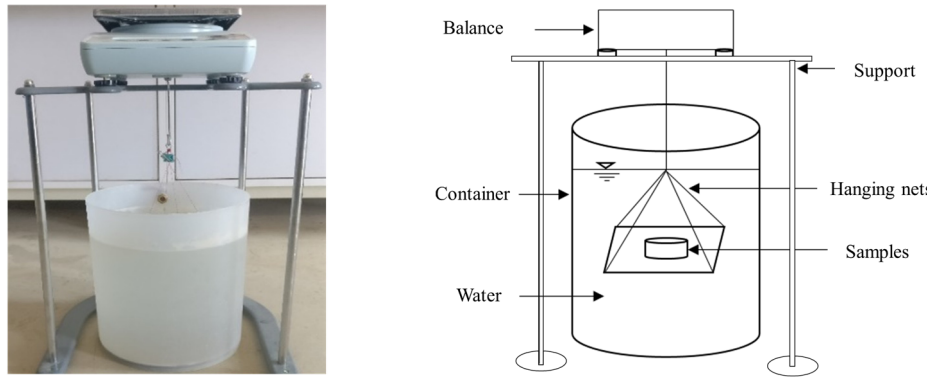


a) Appearance of test set-up b) Sketch of disintegration test

**Fig. 5.** Diagram of disintegration test apparatus. Photo by Jiao Yiwei, Lanzhou University Laboratory, Gansu Province, China, June 10, 2025.

### 3.4. Desiccation tests

The air-dried saline soil was crushed and passed through a mesh sieve with 2 mm in opening. The air-dried soil was placed in a mixing bowl, and 0, 0.2, 0.4, 0.6, 0.8 and 1.0 % at mass concentration (wt%) PAM solutions were added into soil. The initial moisture content was 38 %. For desiccation tests, an initial water content of 38 % was used to generate a slurry state, close to or slightly above the liquid limit, so that drying-induced shrinkage and cracking could be clearly monitored from a saturated condition. After 10 min stirring, 80 g or 70 g slurry was poured into a glass dish with diameter 120 mm or 117 mm. The 4 mm thick slurry was sealed with plastic wrap

after 5 min vibration, and allowed to rest for 24 h. Then, the dish was put into an oven to dry at 50 °C. Control relative humidity and airflow via oven parameters to ensure a constant environment for all specimens. The water loss at a constant temperature was weighed at 0 min, 30 min, 1 h and every 1 h till the mass of specimen unchanged within 2 h [27]. The water loss ratio $L$ was calculated by Eq. (4):

$$L = \frac{m_0 - m_t}{M_0} \times 100\%, \tag{4}$$

where $L$ is water loss ratio, $m_0$ is initial mass, $m_t$ is mass at recording time $t$ and $M_0$ is mass of slurry.

## 4. Results and discussion

### 4.1. PAM effects on Atterberg limits

The Atterberg limit represents the boundary moisture content between different consistency state, the physical state of solid, semi-solid, plastic, fluid of soil. The hydration film around clayey particle composes of strongly absorbed water and weakly absorbed water. With increasing the intruded water, the thickness of hydration film increases and absorbed water gradually transforms to free water so as the physical state of soil changes [28].

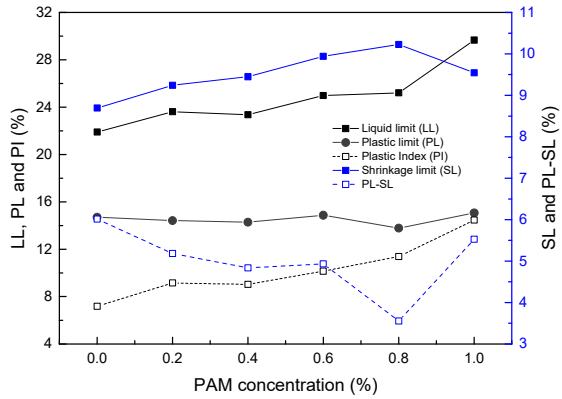


**Fig. 6.** Atterberg limits of PAM treated saline soil

The PLs and LLs of saline soil with different PAM concentration are shown in Fig. 6. The result shows that their LL and plastic index $I_P$ increase, whereas the PL is only slightly increased with increasing the PAM concentration. Soltani-Jigheh et al. (2019) revealed a similar trend that adding PAM leads to an increase liquid limit and plasticity index of high plastic fine grained soil, sampled in Iran, about 26 % and 38 % [16]. Previous research considered that LL is the boundary moisture content of plastic state and fluid state, which is equivalent to the total amount of absorbed water, stern layer and diffuse layer [28]. The PL is the limiting moisture content of semi-solid and plastic state, which is equivalent to the amount of directional binding water in the particle hydration film, stern layer [28]. Barman and Mishra (2022) pointed out that the rise in the cation concentration increased attractive force in bentonite, and the soil structure changed from dispersed to flocculate [21]. Two reasons could explain that soil adsorbs more water when PAM concentration increases. The polymer chain entanglement in PAM solution forms a network structure and confines free water. The active amide group in the molecule forms hydrogen bonds with polar water molecules. Thus, increase of LL and Ip mirror that the weakly adsorbed water volume or thickness of diffuse layer increases. On the other hand, the polymer chain allows free water enter the diffused layer, but restraints it enters the stern layer with strong adsorption

potential. Then, the PL and strongly absorbed water volume are almost unchanged.

The SLs of specimen with different PAM concentrations are shown in Fig. 6. It first increases and then decreases with increase PAM solution concentration. The maximum SL corresponds to 0.8 wt% PAM. Many researchers have studied the significance of the shrinkage limit relating to the geotechnical behavior of soils. As an integral part of Atterberg limits, SL is described as the limiting water content further, which a decrease in water content does not produce any reduction in the volume of soil [21]. Moreover, it represents the limiting moisture content that physical state of soil converts from solid to semi-solid [28]. The results mirror that more water is needed to turn solid state of saline soil to plasticity state, so that PAM polymer strengthens the bond between soil particles. To discuss the strongly adsorbed water further, the parameter of PL-SL, the thickness of stern layer, is also plotted in Fig. 6. It decreases by 2.5 % relative to natural saline soil when 0.8 wt% PAM is added, indicating that the kinetic electric potential of particle surface reduces. The maximum SL value measured under 0.8 % mass fraction PAM conditions, though numerically modest, is marginally higher than adjacent data points and falls within the measurement accuracy range of the SS-1 indenter. It may therefore be regarded as a marginally favourable point.

### 4.2. PAM effects on tensile strength

The tensile strengths of PAM treated soil are shown in Fig. 7. With increase the PAM concentration, the tensile strength determined by Brazilian splitting method decreases, while that by the double punch method increases to a maximum value at 0.8 wt% PAM concentration. It is interesting that the tendency of tensile strength changed with PAM concentration is different in Brazilian splitting and double punch test. Brazilian splitting test is an easy and indirect method for measuring tensile strength of brittle materials, including rocks and concrete [29]. The stress of soil is assumed to be constant along the diameter in accordance to the elastic theory. Double punch test usually gives lower tensile stress compared to the Brazilian due to the fact that the plane of failure in the Brazilian test is predetermined [25], being accordance to the results shown in Fig. 7. On the other side, the undrained strength of clays has been widely related to the liquidity index $I_L$, defined by Eq. (5):

$$I_L = \frac{w - PL}{LL - PL} \times 100\%, \tag{5}$$

where $w$ is the natural water content. Vardanega and Haigh (2014) proved that logarithmic liquidity index correlated with the logarithm of undrained shear strength [30]. The liquidity index (LI) changed with PAM concentration is plotted in Fig. 7, indicating that tensile strength increases with PAM solution adding is more realistic. The liquidity index (LI) employed is recalculated based on water content derived from tensile testing. Consequently, it serves as a standardised metric for interpreting laboratory strength trends rather than directly reflecting in-situ moisture conditions at the construction site.

Then, the reasons attributed to tensile strength results are summarized as below. Firstly, Eq. (1) used in Brazilian splitting test is based on the elastic theory, while Eq. (2) used in double punch test is based on the plastic theory. The remolding water content is larger than PL, so that the double punch method is in line with plastic assumption. Secondly, the amide group in PAM molecular chain forms an attractive hydrogen bond with water molecule, and the polymer chain and the soil particle entangle and crosslink to form a network structure. After 7 days curing, specimens containing PAM solution retains more moisture than specimens without PAM solution, resulting in plastic characteristics of soil. Under the assumption of linear elasticity, the Brazilian splitting test induces a nearly uniform tensile stress along the central diameter of the specimen. In contrast, the double-punch test generates a more complex stress field characterized by a localized compression zone beneath the loading plates and an annular tensile region governed by plastic deformation mechanisms. The specimens in this study were compacted under conditions where

the moisture content exceeded the plastic limit and subsequently underwent sealed curing treatment. The incorporation of polyacrylamide (PAM) significantly enhanced the ductility of the modified soil compared to its untreated counterpart, resulting in a material with superior deformation resistance. Consequently, the double-punch method, rooted in plastic theory, provides a more accurate representation of the actual deformation behavior of PAM-modified soils, particularly under conditions where nonlinear elastic or plastic responses dominate. It is crucial to emphasize that the Brazilian test is rigorously valid only for brittle elastic materials. When the specimen behavior deviates from the pure elastic assumption – as is the case with PAM-modified soils exhibiting increased ductility – this method may underestimate the true tensile strength of the specimens. The observed monotonic decline in Brazilian tensile strength with increasing PAM content can thus be attributed to the combined effects of non-ideal stress distribution and localized compression beneath the loading rods, which become more pronounced as soil ductility increases. In stark contrast, the double-punch test reveals that the peak performance at 0.8 % PAM content aligns consistently with liquid limit index analysis, indicating an optimal balance between cohesive strength and ductility. This finding underscores the superiority of the double-punch method in capturing the nuanced interplay between material properties and deformation mechanisms in PAM-modified soils, particularly when compared to traditional elasticity-based approaches like the Brazilian test.

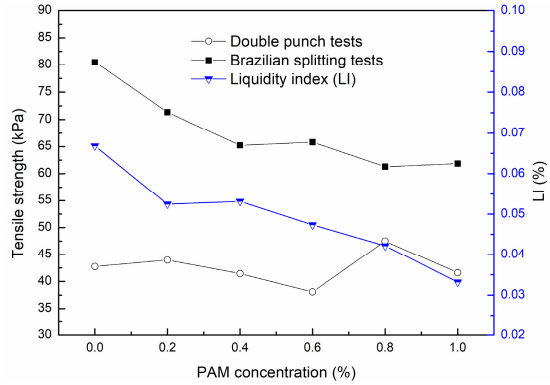


**Fig. 7.** Tensile strengths of PAM treated saline soil

### 4.3. PAM effects on disintegration

The disintegration or dispersion of soil in water is used to evaluate its stability of structure. After soil is immersed in water, the water intrudes into pores, and the air is confined in pores or excluded. With increasing the thickness of particle hydration film, soil swells accordingly. When the swelling pressure generated by compression of closed air and thickening of hydration film breaks the particle connection, the soil structure is destructed [31]. Many factors affecting the disintegration of soil include the mineral composition, particle size distribution, moisture content, chemical composition and concentration of aqueous solution. Larger amount of clay minerals increases the hydration film thickness, so that soil is easier to disintegrate. The particle size distribution determines the porosity and permeability of soil, influencing the disintegration time and disintegration characteristics. Previous research proposed that natural soil at a moisture content smaller than a limited value is relatively stable when sink in water. The concentration of aqueous solution influences the thickness of hydration film, so as the disintegration performance of soil [32].

As shown in Fig. 8, the curve of cumulative disintegration ratio changed with elapsed time is ‘S’ shape. It could be divided into three stages, AB, BC and CD. At stage AB, soil adsorbs water and air in pores is extruded or sealed. Then, soil disintegrates with an almost constant velocity at stage BC, and dispersed soil particle makes water become turbid. At stage CD, the disintegration

process is finalized, and a large amount of sealed air is extruded. Results show that the process of disintegration extends with increase the PAM concentration. When PAM concentration is 0 wt%, the end of disintegration is ~6.0 min. With 1.0 wt% PAM solution, the ending time is about 9.0 min. Moreover, the slope of BC straight segment gradually decreases by adding PAM solution, indicating that the disintegration velocity decreases. The images of samples at different stages are also presented in Fig. 9. When the sample is immersed in water for 1.0 min, the edge of samples with 0, 0.2 and 0.4 wt% PAM is eroded, whereas that with 0.6, 0.8 and 1.0 wt% is relatively intact. At the ending stage, sample with 0 wt% PAM is completely dispersed. While, the core part of samples with ~0.6 wt% PAM is visible.

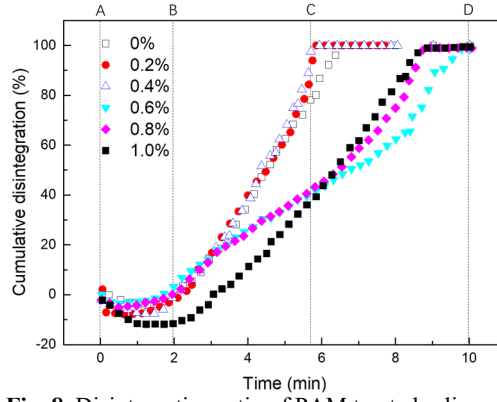


**Fig. 8.** Disintegration ratio of PAM treated saline soil

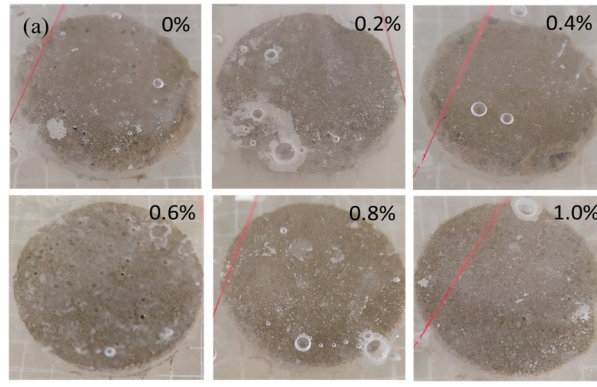


a) Stage AB after 1 min

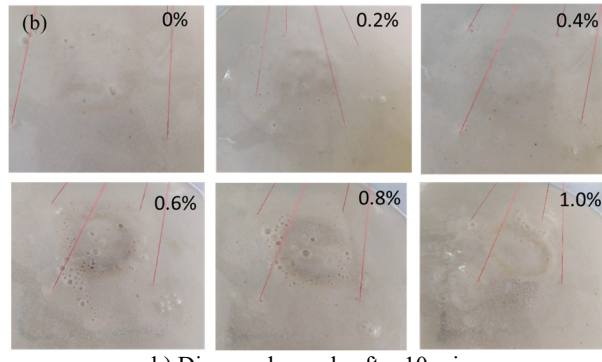


b) Dispersed sample after 10 min

**Fig. 9.** Disintegration process of samples. Photo by Jiao Yiwei, Lanzhou University Laboratory, Gansu Province, China, June 17, 2025


ISSN PRINT 2335-2124, ISSN ONLINE 2424-4635

The above findings indicate that the stability of saline soil in water is improved by PAM treating. Firstly, PAM interacted with components in soil through amide groups to enhance the interparticle bonding. Secondly, the kinetic electric potential of particle surface reduces the swelling pressure [33]. Thirdly, polymer chain adsorbs and bridges soil particles, and enhances the interparticle forces [19].

### 4.4. PAM effects on evaporation

Evaporation of water induces cracks in soil. This process is dependent on chemical composition, physical and mechanical properties and microstructure of soil, determining the formation and development of crack [6]. During water loss of soil, the hydration film on the particle surface gradually attenuates, the interparticle force changes, and particles are rearranged and close to each other [11]. When the shrinkage stress reaches tensile strength, soil cracks develop. The shrinkage volume and cracking behavior correlates to water loss [35]. Tang et al. (2011) investigated the evaporation rate effects on the shrinkage cracking process of initially saturated Romainville expansive soil [7]. However, effect of PAM concentration on water loss is still unknown.

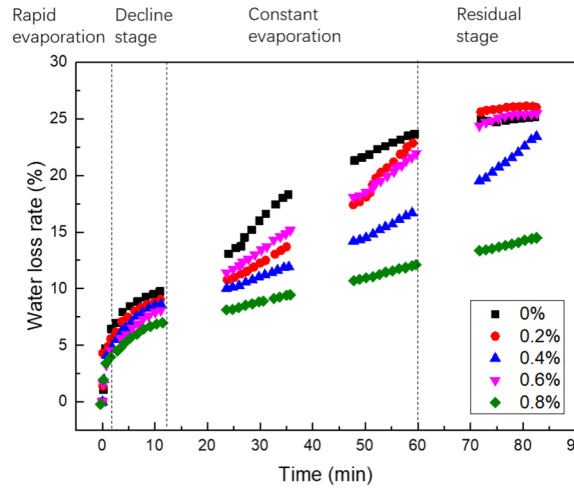


a) Diameter of 120 mm

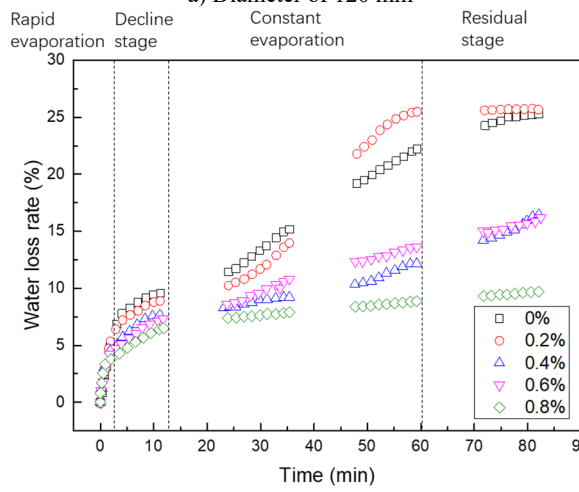


b) Diameter of 117 mm

**Fig. 10.** Water loss rate of slurry samples

The water loss rate of PAM treated soil changed with elapsed time is shown in Fig. 10. The curve could be divided into four stages: rapid evaporation, decline stage, constant evaporation, and residual stage. In rapid evaporation stage, water loss rate linearly relates to drying time. Adding PAM solution cuts the duration of this stage. The duration of rapid evaporation of samples with 0 and 0.2 wt% is 3 h, and that of samples with 0.4, 0.6 and 0.8 wt% is 2 h. In decline stage, the water loss ratio decreases with increasing PAM concentration. During constant evaporation stage, the slope of water loss curves significantly decreases by PAM adding. In the residual stage, PAM treated soil confines more water. The PAM concentration effect is similar for different evaporation surface area. In Fig. 11, the flocculation and agglomeration property of PAM is confirmed at initial mixing stage, which results in viscosity increasing tendency of slurry. With time elapsing and removing of air from the soil, small holes and white bulges appear on the surface of 0 % PAM specimen. After 72 h, the surface of specimen begins to be salted, and the white salted area of 0 % PAM soil is larger than 0.8 % PAM treated soil. Based on the raw data in Fig. 10, we fitted the linear slopes (units: g $h^{-1}$) for each PAM concentration treatment group (0 %, 0.1 %, 0.5%, 1.0% w/v) during the constant evaporation phase (5-15 hours). The $R^2$ value was calculated using the least squares method to assess the goodness of fit. The $R^2$ values for all groups exceeded 0.97, indicating highly reliable linear fits. The horizontal time axis in Fig. 10 terminates at 90 minutes, at which point the slope effectively approaches zero [34].

Two reasons attributes to the results. The amide group on the PAM molecular chain forms hydrogen bonds with polar water molecules, which strengthens the connection and confines water escape from particle surface. PAM reduces the kinetic potential of hydration film, so as the volume change in drying process decreases [35]-[36].

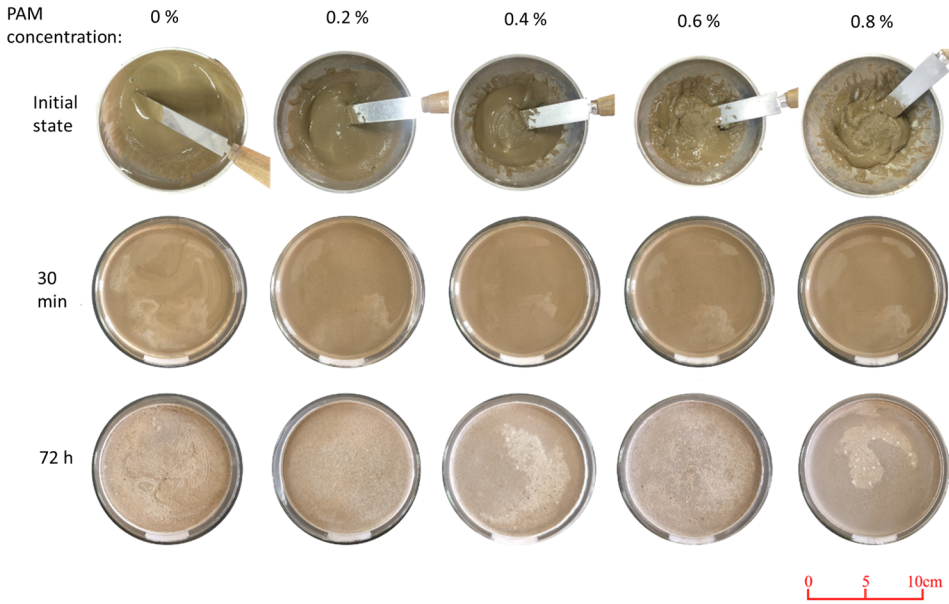


**Fig. 11.** Drying process of slurry samples. Photo by Jiao Yiwei in the laboratory of Lanzhou University, Gansu Province, China on June 27, 2025

PAM (Polyacrylamide) exhibits two distinct bridging effects: one occurs between PAM molecules and clay soil particles, while the other manifests among PAM chains themselves. By facilitating connections between clay soil particles, PAM induces flocculation, and the bridging interactions among PAM chains further enhance the stability of the resulting flocs. Upon addition to clayey soil, the long molecular chains of PAM endow it with a substantial adsorptive surface area in aqueous environments. These chains bind to soil particles, aggregating smaller particles


ISSN PRINT 2335-2124, ISSN ONLINE 2424-4635

into larger, more stable aggregates, thereby reinforcing the structural integrity of clayey soils. From a chemical structural perspective, PAM features polar functional groups within its molecular architecture. Excessive application of PAM, however, can invert the negative surface charge of clay soil particles to a positive charge, thereby increasing electrostatic repulsion forces [37]. Furthermore, the high local concentration of PAM surrounding clay particles disrupts their binding with PAM polymer chains, consequently diminishing the flocculation effect. Unlike other ionic modifiers, PAM is characterized by its long molecular chains and linear structure. One end of a PAM polymer chain attaches to the surface of a clay particle, while the other end forms a bridge with adjacent particles through physical interactions, thereby augmenting both van der Waals forces and electrostatic attractions between clay particles [38]. The adsorption of particles by PAM chains, coupled with chemical entanglement or bonding, results in the formation of a "particle-PAM-particle" network that consolidates dispersed particles into larger aggregates. Additionally, the $–NH_2$ groups in PAM form hydrogen bonds with water molecules, creating a macromolecular structure that restricts molecular motion.

## 5. Conclusions

In this paper, PAM concentration effect on water retention and tensile strength of a saline soil sampled in Dunhuang, China, is explored by Atterberg limits, tensile strength, disintegration and desiccation tests. The main findings are summarized as follows:

1) With increase PAM solution concentration, the liquid limit and plasticity index of saline soil increase, and the plastic limit is almost unchanged. The shrinkage limit first increases and then decreases, and the maximum corresponds to 0.8 wt% PAM.

2) Different tensile strength tests impact on the results. The results determined by Brazilian splitting method shows that the tensile strength decreases with PAM concentration. While the results measured by double punch method reaches to a maximum corresponding to 0.8 wt% PAM. Based on liquid index analysis, the double punch method is recommended.

3) PAM effectively improves water stability of saline soil. As the concentration of PAM solution increases, the disintegration rate slows down and the completion time of dispersion extends.

4) The water retention increases with increase of PAM concentration. The water loss rate in rapid evaporation stage, decline stage and constant evaporation stage in drying process significantly decreases with higher PAM concentration.

5) The active amide group in the molecule forms hydrogen bonds with polar water molecules, enhancing the interparticle bonding. The polymer chain entanglement in PAM solution forms a network structure, confines free water and bridges soil particles. The kinetic electric potential of particle surface reduces the swelling and contraction pressure. Subsequent research will employ micro-scale testing to directly validate the role of these mechanisms within the specific saline-alkali soils examined in this study. Moreover, systematic investigations into the performance of polyacrylamide under varying pore water chemistry conditions and depth-dependent salinity distributions represent a significant avenue for future research.

## Acknowledgements

This study was supported by Gansu Road and Bridge Construction Group Co., Ltd. This study is supported by the project "Application of Water and Salt Separation Technology Based on Soil Hydrophobic Modification in Power Transmission and Transformation Engineering" (Contract No.: SGGSJSOOXMJS2500069).

## Data availability

The datasets generated during and/or analyzed during the current study are available from the

corresponding author on reasonable request.

## Author contributions

Wei Li: experimental scheme planning, experimental data processing, draft writing. Youcai Cao, Yuanhao Li and Quan Wang: experimental data analysis and processing, first draft correction. Yali Wang and Jian Yang: experimental data processing. Yiwei Jiao: final draft writing.

## Conflict of interest

The authors declare that they have no conflict of interest.

## References

**[1]** X. Wei, M. Hattab, S. Taibi, K. V. Bicalho, L. Xu, and J.-M. Fleureau, "Crack development and coalescence process in drying clayey loess," (in Chinese), *Geomechanics and Engineering*, Vol. 25, No. 6, pp. 535–552, Jan. 2021, https://doi.org/10.12989/gae.2021.25.6.535

**[2]** R. Q. Zeng et al., "Characterizing hydrological processes on loess slopes using electrical resistivity tomography – A case study of the Heifangtai Terrace, Northwest China," *Journal of Hydrology*, Vol. 541, pp. 742–753, Jul. 2016, https://doi.org/10.1016/j.jhydrol.2016.07.033

**[3]** B. A. Albrecht and C. H. Benson, "Effect of desiccation on compacted natural clays," *Journal of Geotechnical and Geoenvironmental Engineering*, Vol. 127, No. 1, pp. 67–75, Jan. 2001, https://doi.org/10.1061/(asce)1090-0241(2001)127:1(67)

**[4]** O. S. Baghabra Al-Amoudi and S. N. Abduljauwad, "Compressibility and collapse characteristics of arid saline sabkha soils," *Engineering Geology*, Vol. 39, No. 3-4, pp. 185–202, Jun. 1995, https://doi.org/10.1016/0013-7952(95)00016-9

**[5]** B.-L. Gan, D.-M. Zhang, Z.-K. Huang, F.-Y. Zheng, R. Zhu, and W. Zhang, "Ontology-driven knowledge graph for decision-making in resilience enhancement of underground structures: Framework and application," *Tunnelling and Underground Space Technology*, Vol. 163, p. 106739, Sep. 2025, https://doi.org/10.1016/j.tust.2025.106739

**[6]** C. Tang, B. Shi, C. Liu, L. Zhao, and B. Wang, "Influencing factors of geometrical structure of surface shrinkage cracks in clayey soils," *Engineering Geology*, Vol. 101, No. 3-4, pp. 204–217, Oct. 2008, https://doi.org/10.1016/j.enggeo.2008.05.005

**[7]** C.-S. Tang, B. Shi, C. Liu, W.-B. Suo, and L. Gao, "Experimental characterization of shrinkage and desiccation cracking in thin clay layer," *Applied Clay Science*, Vol. 52, No. 1-2, pp. 69–77, Apr. 2011, https://doi.org/10.1016/j.clay.2011.01.032

**[8]** P. H. Morris, J. Graham, and D. J. Williams, "Cracking in drying soils," *Canadian Geotechnical Journal*, Vol. 29, No. 2, pp. 263–277, Apr. 1992, https://doi.org/10.1139/t92-030

**[9]** H. Peron, T. Hueckel, L. Laloui, and L. B. Hu, "Fundamentals of desiccation cracking of fine-grained soils: experimental characterisation and mechanisms identification," *Canadian Geotechnical Journal*, Vol. 46, No. 10, pp. 1177–1201, Oct. 2009, https://doi.org/10.1139/t09-054

**[10]** P. Yin and S. K. Vanapalli, "Model for predicting tensile strength of unsaturated cohesionless soils," *Canadian Geotechnical Journal*, Vol. 55, No. 9, pp. 1313–1333, Sep. 2018, https://doi.org/10.1139/cgj-2017-0376

**[11]** C.-S. Tang et al., "Desiccation cracking of soils: A review of investigation approaches, underlying mechanisms, and influencing factors," *Earth-Science Reviews*, Vol. 216, p. 103586, May 2021, https://doi.org/10.1016/j.earscirev.2021.103586

**[12]** P. Yu, X. Wang, J. Yu, Y. Yu, and H. Lv, "XFEM Simulation of soil crack evolution process considering the stress concentration and redistribution at the crack tip," *International Journal of Geomechanics*, Vol. 22, No. 9, Sep. 2022, https://doi.org/10.1061/(asce)gm.1943-5622.0002505

**[13]** T. Zhang, Y. Deng, Y. Cui, H. Lan, F. Zhang, and H. Zhang, "Porewater salinity effect on flocculation and desiccation cracking behaviour of kaolin and bentonite considering working condition," *Engineering Geology*, Vol. 251, pp. 11–23, Mar. 2019, https://doi.org/10.1016/j.enggeo.2019.02.007

**[14]** F. W. Barvenik, "Polyacrylamide characteristics related to soil applications," *Soil Science*, Vol. 158, No. 4, pp. 235–243, Oct. 1994, https://doi.org/10.1097/00010694-199410000-00002

**[15]** G. J. Levy and W. P. Miller, "Polyacrylamide adsorption and aggregate stability," *Soil and Tillage Research*, Vol. 51, No. 1-2, pp. 121–128, Jan. 1999, https://doi.org/10.1016/s0167-1987(99)00048-3

**[16]** H. Soltani-Jigheh, M. Bagheri, and A. R. Amani-Ghadim, "Use of hydrophilic polymeric stabilizer to improve strength and durability of fine-grained soils," *Cold Regions Science and Technology*, Vol. 157, pp. 187–195, Jan. 2019, https://doi.org/10.1016/j.coldregions.2018.10.011

**[17]** D. Yongfeng, L. Songyu, H. Jian'An, L. Kan, D. Yanjun, and J. Fei, "Strength and permeability of cemented soil with PAM," in *Grouting and Deep Mixing 2012*, pp. 1800–1807, Aug. 2012, https://doi.org/10.1061/9780784412350.0155

**[18]** R. N. Georgees, R. A. Hassan, R. P. Evans, and P. Jegatheesan, "Resilient response characterization of pavement foundation materials using a polyacrylamide-based stabilizer," *Journal of Materials in Civil Engineering*, Vol. 30, No. 1, Jan. 2018, https://doi.org/10.1061/(asce)mt.1943-5533.0002109

**[19]** Q. S. M. Shafiqu, "Effect of adding polyacrylamide polymer with lime and cement kiln dust on the properties of expansive clayey soils," *International Journal of Geomate*, Vol. 15, No. 51, pp. 233–239, Jan. 2018, https://doi.org/10.21660/2018.51.19491

**[20]** J. Xia, S. Zhang, X. Zhao, J. Liu, and Y. Chen, "Effects of different groundwater depths on the distribution characteristics of soil-Tamarix water contents and salinity under saline mineralization conditions," *Catena*, Vol. 142, pp. 166–176, Jul. 2016, https://doi.org/10.1016/j.catena.2016.03.005

**[21]** D. Barman and A. K. Mishra, "Influence of salt and initial conditions on the shrinkage limit of bentonite," *International Journal of Geotechnical Engineering*, Vol. 16, No. 1, pp. 64–73, Jan. 2022, https://doi.org/10.1080/19386362.2019.1684656

**[22]** F. Ming, D. Li, M. Zhang, and Y. Zhang, "A novel method for estimating the elastic modulus of frozen soil," *Cold Regions Science and Technology*, Vol. 141, pp. 1–7, Sep. 2017, https://doi.org/10.1016/j.coldregions.2017.05.005

**[23]** S. Bulolo, E. C. Leong, and R. Kizza, "Tensile strength of unsaturated coarse and fine-grained soils," *Bulletin of Engineering Geology and the Environment*, Vol. 80, No. 3, pp. 2727–2750, Jan. 2021, https://doi.org/10.1007/s10064-020-02073-6

**[24]** B. Li and S. Akhtar, "Characterizations of tensile yield and failure processes of frozen clay soils: laboratory testing and numerical modeling," *Bulletin of Engineering Geology and the Environment*, Vol. 81, No. 10, Sep. 2022, https://doi.org/10.1007/s10064-022-02942-2

**[25]** A. Al Houri, A. Habib, A. Elzokra, and M. Habib, "Tensile testing of soils: history, equipment and methodologies," *Civil Engineering Journal*, Vol. 6, No. 3, pp. 591–601, Jan. 2020, https://doi.org/10.28991/cej-2020-03091494

**[26]** X. Liu, X. Zhang, L. Kong, G. Wang, and J. Lu, "Disintegration of granite residual soils with varying degrees of weathering," *Engineering Geology*, Vol. 305, p. 106723, Aug. 2022, https://doi.org/10.1016/j.enggeo.2022.106723

**[27]** C.-S. Tang, Y.-J. Cui, B. Shi, A.-M. Tang, and C. Liu, "Desiccation and cracking behaviour of clay layer from slurry state under wetting-drying cycles," *Geoderma*, Vol. 166, No. 1, pp. 111–118, Jul. 2011, https://doi.org/10.1016/j.geoderma.2011.07.018

**[28]** B. Zhou and N. Lu, "Correlation between Atterberg limits and soil adsorptive water," *Journal of Geotechnical and Geoenvironmental Engineering*, Vol. 147, No. 2, Feb. 2021, https://doi.org/10.1061/(asce)gt.1943-5606.0002463

**[29]** D. Li and L. N. Y. Wong, "The Brazilian disc test for rock mechanics applications: review and new insights," *Rock Mechanics and Rock Engineering*, Vol. 46, No. 2, pp. 269–287, May 2012, https://doi.org/10.1007/s00603-012-0257-7

**[30]** P. J. Vardanega and S. K. Haigh, "The undrained strength – liquidity index relationship," *Canadian Geotechnical Journal*, Vol. 51, No. 9, pp. 1073–1086, Jan. 2014, https://doi.org/10.1139/cgj-2013-0169

**[31]** X. W. Zhang, L. W. Kong, X. L. Cui, and S. Yin, "Occurrence characteristics of free iron oxides in soil microstructure: evidence from XRD, SEM and EDS," *Bulletin of Engineering Geology and the Environment*, Vol. 75, No. 4, pp. 1493–1503, Aug. 2015, https://doi.org/10.1007/s10064-015-0781-2

**[32]** Y. Fang, Y. Yao, T. Song, L. Wei, P. Liu, and B. Zhuo, "Study on disintegrating characteristics and mechanism of cutterhead mud-caking in cohesive strata," *Bulletin of Engineering Geology and the Environment*, Vol. 81, No. 12, Nov. 2022, https://doi.org/10.1007/s10064-022-03018-x

**[33]** X. Kang, B. Bate, R.-P. Chen, W. Yang, and F. Wang, "Physicochemical and mechanical properties of polymer-amended kaolinite and fly ash-kaolinite mixtures," *Journal of Materials in Civil Engineering*, Vol. 31, No. 6, Jan. 2019, https://doi.org/10.1061/(asce)mt.1943-5533.0002705

**[34]** J. J. B. Bronswijk, "Relation between vertical soil movements and water-content changes in cracking clays," *Soil Science Society of America Journal*, Vol. 55, No. 5, pp. 1220–1226, Jan. 1991, https://doi.org/10.2136/sssaj1991.03615995005500050004x

**[35]** Y. Wang et al., "Effects of anionic polyacrylamide on structural characteristics and dissolved organic carbon stability of calcareous soils," *Soil and Tillage Research*, Vol. 255, p. 106825, Jan. 2026, https://doi.org/10.1016/j.still.2025.106825

**[36]** Y.-L. Sun, S.-C. Tu, Z.-P. Xiao, C. Yu, X.-W. Zhang, and Y.-J. Song, "Disintegration characteristics, splitting tensile strength and microscopic mechanisms of marine silty soil improved by PAM and CLS," *Science of The Total Environment*, Vol. 1002, p. 180573, Nov. 2025, https://doi.org/10.1016/j.scitotenv.2025.180573

**[37]** G. Xu et al., "Impact of several sludge dewatering conditioners on municipal sludge pyrolysis properties, kinetics, by-products, and environmental risk assessment," *Science of The Total Environment*, Vol. 951, p. 175653, Nov. 2024, https://doi.org/10.1016/j.scitotenv.2024.175653

**[38]** J. Yang, S. Li, H. Di, D. Liu, X. Wang, and J. Zhao, "Experimental investigations on the physico-mechanical and microstructural properties of loess reinforced with anionic polyacrylamide," *Construction and Building Materials*, Vol. 409, p. 134124, Dec. 2023, https://doi.org/10.1016/j.conbuildmat.2023.134124

**Wei Li** received master's degree. He is now working in the State Grid Gansu Electric Power Company Construction Branch, senior engineer. The main research direction is the construction management of power transmission and transformation projects.

**Youcai Cao** received master's degree. He is now working in the State Grid Gansu Electric Power Company Construction Branch, engineer. The main research direction is the construction of power grid engineering.

**Yuanhao Li** received master's degree. He is now working in the State Grid Gansu Electric Power Company Construction Branch, engineer. The main research direction is the construction of power grid engineering.

**Quan Wang** Bachelor's degree. He is now working in the State Grid Gansu Electric Power Company Construction Branch, senior engineer. The main research direction is the construction management of power transmission and transformation projects.

**Yali Wang** received bachelor's degree. He is now working in the State Grid Gansu Electric Power Company Construction Branch, Senior Economist. The main research direction is the construction management of power transmission and transformation projects.

**Jian Yang** received master's degree. He is now working in the State Grid Gansu Electric Power Company Construction Branch, engineer. The main research direction is the construction of power grid engineering.

**Yiwei Jiao** is a postgraduate student in the School of Civil Engineering and Mechanics, Lanzhou University, China.